THE ASTROPHYSICAL JOURNAL, 430:1–12, 1994 July 20

BIAS PROPERTIES OF EXTRAGALACTIC DISTANCE INDICATORS. I. THE HUBBLE CONSTANT DOES NOT INCREASE OUTWARD

ALLAN SANDAGE
The Observatories of the Carnegie Institution of Washington, 813 Santa Barbara Street, Pasadena, CA 91101
Received 1993 August 31; accepted 1994 January 21

ABSTRACT

Observational selection bias in flux-limited catalogs of field galaxies can be detected using a diagram in which the calculated intrinsic luminosity of each galaxy is plotted against its redshift. Apparent correlations of absolute magnitude with redshift that are not real, but rather are caused by selection effects can be identified by adding a fainter sample. If an apparent correlation is due to bias, it will disappear at the original flux level but will reappear with the same properties near the limit of the fainter catalog. The method is illustrated using S0 + Sa galaxies from two catalogs with different apparent magnitude limits. The demonstration is the same as that made earlier using Sc I galaxies (Sandage 1988a).

To avoid photometric distance determinations that are systematically incorrect as a function of redshift, it is necessary to use mean absolute magnitudes, $M(m, v_i)$, that are functions of the apparent magnitude limit of the catalog, m, and of the observed individual redshifts, v_i. This double-entry $M_0 - M(m, v_i)$ correction to the proper volume-limited absolute magnitude M_0 is calculated and is listed in a table. Failure to apply this bias correction at every redshift will give an incorrect Hubble constant that apparently increases outward. The clue that bias corrections are needed is that the apparent Hubble constant calculated using uncorrected data from two catalogs with different flux limits will be double-valued at a given redshift, one value for each catalog, which is a clear contradiction.

Subject headings: cosmology: observations — distance scale — galaxies: distances and redshifts — methods: statistical

1. INTRODUCTION

The current debate over the value of the Hubble constant will cease only when one or the other of the distance scales is shown to be incorrect. Said differently, a decisive case must eventually be made against one scale, in addition to experiments made in support of the other. No matter how strong an experiment may eventually be mounted for one or the other of the scales, the incorrect supporting explanations for the faulty scale will continue to be cited as contrary evidence. There are, of course, a few cases where a new experiment has been so overwhelming that it closed a problem without question, but such guillotines are rare. The prime example is Hubble's discovery of Cepheids in M31 that disproved van Maanen's claims of measured proper motions for the M31 stellar content. A refutation of the proper-motion data was unnecessary after the Cepheid fact.

Although panegyrics defending favored methods exist in abundance, no criticisms are yet strong enough to satisfy either side for or against the long or the short extragalactic scale. Judged by their effect, the several summary critiques of the short scale (Tammann 1986, 1987, 1991, 1993; Tammann & Sandage 1982; Sandage & Tammann 1976, 1990; Sandage 1993a, b) were adumbrations before their time. Furthermore, specific discussions of the bias properties of flux-limited Tully-Fisher (TF) samples, both for the Virgo Cluster (Kraan-Korteweg, Cameron, & Tammann 1986, 1988) and for field galaxies (Sandage 1988b), have also been either insufficiently explicit or too misunderstood to be noticed. Similar discussions by Bottinelli et al. (1986a, b, 1988) and Teerikorpi (1975a, b, 1984, 1987, 1990) also reach the conclusion that the long distance scale is correct when a proper accounting is made for the bias properties of the sample. These papers have not closed the debate either.

The purpose of this and later papers in this series is to begin critiques showing why particular methods, applied without selection bias corrections, give incorrect distance scales. Our position is that observational selection bias holds part of the answer as to why certain methods give incorrect results.

We begin by developing procedures to account for selection bias when using photometric distance indicators. The methods developed in this and the following several papers appeal to the intuition in ways that differ from the profound respect and consequent awe associated with that subset of the methods among the esoteric mathematical models that have an impractical felicity.

In this first paper we set out a direct method to identify selection bias in any sample of objects of the same "type" that have been selected by apparent magnitude. For illustration we use the complete flux-limited sample of S0 + Sa galaxies in the Revised Shapley-Ames catalog (Sandage & Tammann 1981, 1987, hereafter RSA1, RSA2). The method extends an earlier discussion using Sc I galaxies (Sandage 1988a) taken from three catalogs with different apparent magnitude limits.

The method centers around what we call the *Spaenhauer diagram*, where absolute magnitudes calculated from redshifts

are plotted against relative distances.[1] We show that this provides powerful and sufficient information to determine the bias corrections directly, nothing else being needed. The principle is that adding a fainter sample shows the presence of bias, if it exists.

The more complicated case is treated in the following paper (Sandage 1994, hereafter Paper II), where flux-limited samples of objects of multiple "types" are used with the TF line-width method to determine individual "distance." In this case, each "type" corresponds to a discrete bin of *line width*. It is shown there that the correction for the effects of bias changes the apparent short distance scale into the long scale when the corrections are individually applied at each redshift and now at *each line width* as well.

For illustration, the method is applied in Paper II to a particular TF catalog in the literature (Aaronson et al. 1982) to show that the Hubble constant is multivalued, depending on the line width and the redshift, unless the triple-entry bias corrections determined from the data themselves are applied.

Federspiel, Sandage, & Tammann (1994, hereafter Paper III or FST94) apply the methods to the 1355 TF galaxy sample of Mathewson, Ford, & Buchhorn (1992), which is so large that it can be divided into separate catalogs with different apparent magnitude limits, redshift intervals, line widths, and positions relative to the direction of the dipole of the microwave background. All the bias properties predicted from the model are seen in remarkable detail in this large sample. Again it is shown that if the triple-entry bias corrections are not applied to these data, then incorrect conclusions will be made concerning (1) the reality of the apparent increase in the Hubble constant outward, (2) the value of H_0, and (3) the nature of streaming motions superposed on a smooth Hubble flow. In particular, we show in Paper III that the details of the Great Attractor and the 500 km s^{-1} offset relative to the kinematic frame of the CMB in the restricted direction of the CMB dipole for relatively local galaxies ($v < 4000$ km s^{-1}) are modified when the data are corrected for selection bias.

[1] The procedure assumes a strictly linear redshift-distance relation, with no account taken of a velocity scatter in the observed redshifts about the cosmological value caused by random and/or streaming motions. We argue as follows that kinematic distances based on redshifts are considerably more accurate than photometric distances based on most of the "standard candles," and therefore most claims of streaming motions are incorrect that are based on comparing individual redshift and photometric distances.

It is shown here (see footnote 3 below) and in Paper II of this series (Sandage 1994, § 2.2), and earlier by numerical experiments (Kraan-Korteweg, Sandage, & Tammann 1984; Sandage 1988b), that the $\sigma(M)$ values calculated with and without the correction for the Virgo streaming perturbation (the so-called Virgo infall) are virtually the same. Hence, the Virgo perturbation has a nearly negligible effect on $\sigma(M)$ determined using redshift distances.

The streaming motion related to the cosmic microwave background (CMB), which, of course, is real, is also a second-order effect, producing only a constant offset to kinematic distances, not a systematic error with distance, because, in first approximation, the local region (i.e., with $v < 4000$ km s^{-1}) is moving in bulk toward the hot CMB pole (see § 2.2 of Paper II).

Therefore, only *random* motions need be considered in assessing the relative accuracy of distances by redshifts and by photometric indicators. These are discussed in Paper II (§ 2.2) with the conclusion that the spurious $\sigma(M)$ due to $\Delta v_{\rm random}$ velocities is, at most, 0.3 mag which is small compared with $\sigma(M) \gtrsim 0.7$ mag for most photometric indicators. This argument is made by noting that errors in kinematic distances due to even the grossest assumption that $\sigma(v)_{\rm random} \sim 200$ km s^{-1} are less than the stated 0.3 mag.

It is on this precept that kinematic absolute magnitudes are superior to photometric distances that we base the method developed in this series to find the bias properties of any sample. The principle is to compare kinematic and photometric distances, transformed to absolute magnitudes, to search for systematic differences with redshift for the latter.

It is emphasized in these papers that the basic correction discussed and applied here is not the classical Malmquist (1920) correction (see Bok 1937, p. 17, and Mihalas & Binney 1981 for derivations), which is only the difference between the volume-limited mean absolute magnitude, M_0, and the ensemble mean absolute magnitude, $M(m)$, of the complete flux-limited sample. Rather, the correction to M_0 is a double-entry correction, $M(m, v_i)$, needed at *every redshift*. For the TF method discussed in Paper II we need a triple-entry correction at every redshift, at every line width, and for any value of the apparent magnitude limit of a particular catalog.

We show in the next section that the $M(m)$ mean absolute magnitude calculated by Malmquist (1920) is the value of the individual $M(m, v_i)$ corrections averaged over all redshifts; the needeed individual $M(m, v_i)$ corrections are thereby lost. The distinction between $M(m)$ and $M(m, v_i)$ is important, and the purpose of this paper is to develop the difference between these two concepts.

The problem is introduced in the next section, where it is shown that the difference of the slope of the Hubble diagram for field galaxies from its expected value of d mag/d log $z = 5$ is due to the progressive selection bias with increasing distance. A calculation of the individual corrections, $M_0 - M(m, v_i)$, is set out in § 3 for each distance interval and for any particular arbitrary apparent magnitude cutoff m. The effect of adding a fainter sample to identify the presence of bias is illustrated in the penultimate section.

We show in the final section that neglecting the bias which is progressive with redshift leads to the incorrect conclusion that the Hubble constant increases outward (de Vaucouleurs & Peters 1986; Tully 1988; Giraud 1985, 1986a, b, c).

2. BIAS PROPERTIES OF THE S0 + Sa GALAXY SAMPLE FROM THE RSA

2.1. *The Spaenhauer Diagram*

An illustration of observational selection bias of flux-limited samples is shown in Figure 1, taken from an earlier study (Sandage 1972b). Plotted as ordinate is the absolute radio power emitted by 59 radio galaxies, 103 radio-loud quasars, and 25 radio-quiet quasars that appear in three different radio catalogs. The abscissa values are calculated as distance moduli from the redshifts using $m - M = 5 \log z + 48.88$, based on $H_0 = 50$ km s^{-1} Mpc^{-1} and $q_0 = 1$. Note that the abscissa data depend only on the observed redshift, not on assumptions about bias.

The radio sources are all from strictly flux-limited catalogs. The 3C catalog has a limit of 9 Jy at 178 MHz, the 4C at 2 Jy, and the Parkes sources at 7.1 Jy when reduced to the fiducial frequency of 178 MHz using a spectral index of 0.7. Hence, the contents of these catalogs are highly biased, containing only the several hundred apparently brightest radio sources that exist.

The bias properties here are similar to those of, say, the Bright Star Catalogue (Hoffleit 1982). No M dwarfs exist in that catalog because their absolute magnitudes are so faint that none are close enough to be included in a catalog whose grasp is only to apparent magnitude $V \sim 6.5$.

Figure 1 shows this point directly for radio sources by noting that the average absolute magnitude of the catalog entries becomes brighter with increasing distance, even through the true (physically correct) average absolute magnitude, M_0, for a volume-limited sample is constant. Clearly the

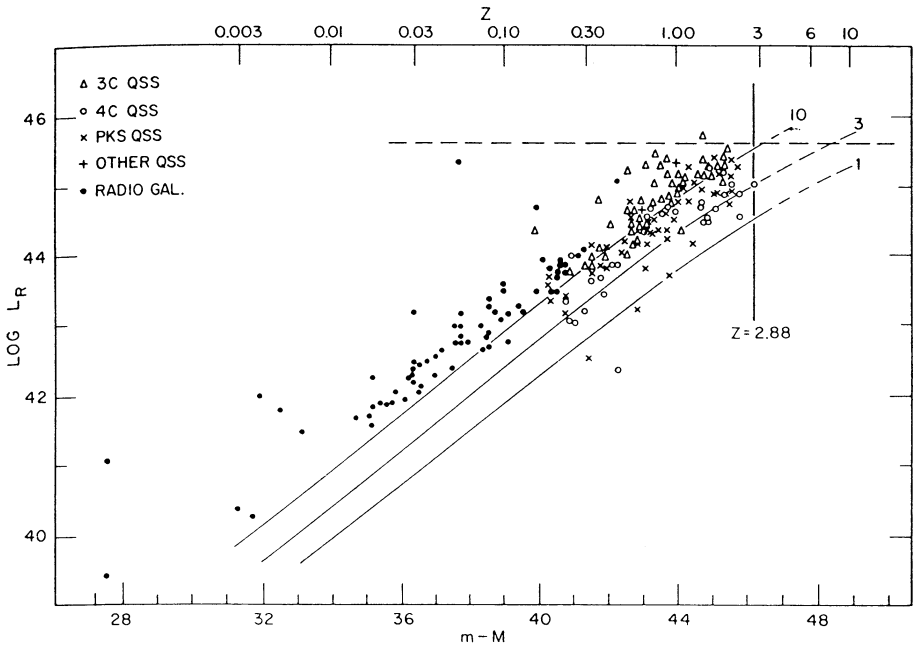

FIG. 1.—"Spaenhauer" diagram for radio sources identified from the 3C, 4C, and Parkes surveys that are strictly flux-limited. The relative distance moduli along the abscissa depend only on the observed redshift. The ordinate is absolute radio power in ergs s^{-1}, integrated over the radio band from 10^7 to 10^{11} Hz, calculated from the redshifts using $H_0 = 50$ km s^{-1} Mpc^{-1} and $q_0 = 1$. Lines of constant apparent flux are shown. The diagram is from Sandage (1972b).

corrections $M_0 - M(m, d_i)$ at any true distance, d_i, increase with d_i. This is the correction we seek.

An interpretation of the apparent correlation of L_R (the absolute radio power) with redshift in Figure 1 could have been that the intrinsic power of the radio sources actually does vary with distance, approximately as $L_R \sim z^2$. However, as soon as the lines of fixed apparent flux are drawn as shown, it is clear that only the tip of the intrinsic luminosity function is sampled, due to the strict flux limitation of each catalog.

Because of the very broad luminosity function that spans a factor of $\sim 10^6$ in L_R, and also because of the steepness of the luminosity function at the bright end, the observed points hug the flux limit lines of each respective catalog. (These limit lines are slightly curved in Fig. 1 because the K-correction has been applied, accounting for the effects of redshift; see Sandage 1972b, eqs. [4]–[6], for details.)

Because the variation of L_R with redshift is so pronounced in Figure 1, there was never any doubt that its interpretation was a selection effect; the mean radio power of sources does not in fact vary as z^2, although other interpretations of Figure 1 could rationally have been made in the absence of other data.

A. It could be argued that the apparent increase of absolute luminosity with redshift is not real, or in fact due to bias, but is rather an artifact of a *faulty* calculation of L_R using an incorrect redshift-distance relation (the Hubble linear law here). If we had, instead, made the calculation using a "correct" redshift-distance relation, we could have removed[2] the apparent variation of L_R (calculated) with z.

[2] However, the case of $L_R \sim z^2$ is degenerate to the possibility of a *total* removal of the apparent correlation in Fig. 1 by changing the form of the redshift-distance relation. To obtain a complete lack of an $L(z)$ dependence when the apparent dependence is $L_R \sim z^2$, as in Fig. 1, requires that redshift not be correlated with distance at all. However, in the cases where the calculated correlation of absolute luminosity with redshift is less steep than z^2, it is always possible to devise a redshift-distance relation, nonphysical though it may be, that would reduce or remove entirely the apparent correlation of luminosity with redshift.

Segal's (1982) analysis of the Hubble diagram of field galaxies and quasars does just that. He adjusts a nonlinear redshift-distance law (a square law in his case) to fit the observed (apparent) slope of the Hubble diagram, but then he requires a very narrow luminosity function—essentially a delta function.

However, his explanation is contrived. Independent data from clusters show beyond doubt that a broad galaxian luminosity function exists (Kraan-Korteweg et al. 1984; Binggeli, Sandage, & Tammann 1988). There necessarily, then, will be selection bias for the reasons discussed here and elsewhere (Sandage, Tammann, & Yahil 1979, hereafter STY79; Sandage 1988a, b, hereafter S88a, S88b) when using flux-limited samples. And there is, of course, decisive independent evidence that the redshift-distance relation is linear (except for local streaming motions superposed on the underlying linear expansion field; see Paper III), proved at a level better than $\pm 2\%$ using precise distance ratios (Sandage 1972a, 1975, Figs. 4 and 5; Sandage & Hardy 1973; Sandage & Tammann 1975, Fig. 6; Sandage 1992; Lauer & Postman 1992; Sandage & Tammann 1993; Jerjen & Tammann 1993).

We showed elsewhere (STY79; S88a), and show again here, that the case of true bias, rather than a failure of the linear redshift-distance relation, can be disproved by adding a fainter sample. Figure 1 illustrates the point by noting the positions of the three progressively fainter flux limit lines. The data hug each fainter line as the fainter data are added. Modern data, reaching flux levels 1000 times fainter than the 1 Jy line in Figure 1, confirm that the entire region of Figure 1 is filled between the 9 Jy limit line of the 3C catalog and such a 1 mJy limit line (not shown). This is the proof that the observed apparent correlation in Figure 1 is due to selection bias rather than being a true correlation.

B. Similar apparent increases of some intrinsic property with z as in Figure 1 have sometimes been claimed to be due to a real change of that property (i.e., due to evolution) in the lookback time corresponding to that redshift. Again, adding a

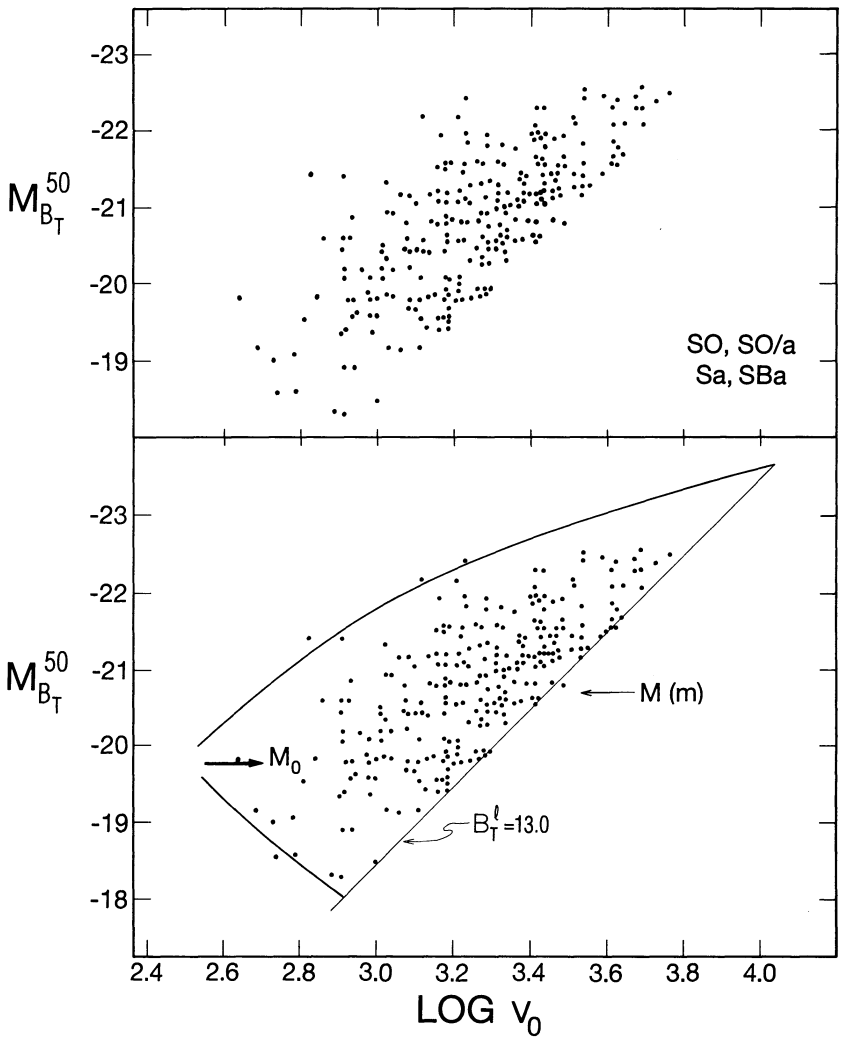

FIG. 2.—*Top*: Apparent variation of absolute magnitudes for the complete sample of S0 and Sa galaxies in the flux-limited RSA Catalog, calculated from the redshift using $H_0 = 50$ km s^{-1} Mpc^{-1}. *Bottom*: Same as top, but with upper and lower envelope lines superposed from Fig. 3 and showing the flux-limit line at $B_T = 13$. The apex magnitude, M_0, is the most probable mean absolute magnitude of the luminosity function. The ensemble mean absolute magnitude, $M(m)$, for the complete flux-limited sample is shown by the arrow. The difference between M_0 and $M(m)$ is the gross Malmquist correction for the total sample, integrated over all redshifts.

fainter sample and seeing the alleged effect move faintward by 1 mag for each 0.2 dex in redshift proves the case for bias rather than the signature of an intrinsic effect.

Hence, diagrams such as Figure 1 (absolute luminosity versus some measure of distance) provide powerful diagnoses by which to identify bias problems in flux-limited samples. We adopt as the eponymous name for the generic diagram that of Spaenhauer (1978), who introduced it in his solutions to particular problems of Galactic structure.

2.2. *The Spaenhauer Bias Diagram for RSA S0 + Sa Galaxies*

Figure 2 (*top panel*) shows the Spaenhauer diagram for a complete sample of S0 + S0/a, Sa, and SBa galaxies from the flux-limited RSA2 catalog. The redshift, reduced to the centroid of the Local Group, is taken from column (20) of that catalog and is plotted as abscissa. The absolute magnitudes for the ordinate are calculated from the listed B_T apparent magnitudes using v_0 redshifts[3] and a Hubble constant of $H_0 = 50$ km s^{-1} Mpc^{-1}.

The apparent increase of luminosity with redshift in Figure 2 (*top*) is nearly identical to that found earlier for the E galaxies (STY79) and, as previously mentioned, for Sc I galaxies (S88a). The sharp edge of the apparent correlation of redshift and luminosity, caused by the apparent magnitude limit at $B_T = 13$, moves to higher redshifts when a fainter sample is added (see Fig. 11 below) rather than continuing the correlation to brighter magnitudes. Therefore, the correlation in the top panel of Figure 2 is not due to the failure of a linear redshift-distance law (Segal 1982), or to an outward increase in the

[3] The calculations were repeated using the redshifts corrected for "Virgo Cluster infall" of 220 km s^{-1} (Tammann & Sandage 1985; Kraan-Korteweg 1986a, b). These gave only negligible differences from the principal features of the top panel of Fig. 2.

Hubble constant (Tully 1988), but is clearly caused by selection bias due to the flux limitation of the RSA.

This point is made in the bottom panel of Figure 2, where limiting-envelope lines are drawn from the known properties of the RSA sample. The curved upper envelope is fitted by eye to the brightest part of the distribution as the redshift increases, based on the analytical expectation of this envelope from Figure 3 (see § 3). The straight line is the locus of the apparent magnitude limit of the RSA at $B = 13$, calculated from $m - M = 5 \log v_0 + 16.5$, which follows from $H_0 = 50$ km s^{-1} Mpc^{-1}.

The apex position at absolute magnitude near $M_0 = -19.8$, marked by the arrow, is the most probable value for the volume-limited mean absolute magnitude. For a luminosity function that is symmetric in magnitudes (i.e., in log L), this would be the mean absolute magnitude of the data points enclosed between the upper and lower envelope lines for redshifts smaller than $\log v_0 = 2.9$. This is the log redshift where the $B_T = 13.0$ apparent magnitude limit line intersects the lower envelope curve. The intersection defines the redshift limit beyond which the sample is no longer volume-limited. It is at this point that the systematic corrections for selection bias must begin for larger redshifts.

The ensemble mean absolute magnitude, $M(m)$, for the *complete* sample enclosed within the three envelope lines in Figure 2 (*bottom*) is shown by the arrow marked $M(m)$. This is the number calculated by Malmquist (1920) in his derivation of $M_0 - M(m) = 1.386\,\sigma^2$ for a Gaussian luminosity function for objects distributed uniformly in space.

However, to correct each object for bias, we need the more complicated progressive corrections, $M_0 - M(m, v_i)$, at each redshift, v_i, for which v_i is larger than the redshift that divides the volume-limited subset of the sample from the flux-limited subset.

The horizontal position (i.e., the redshift) of the apex in the bottom panel of Figure 2 is determined by the normalization of the luminosity function, determined by the volume that must be surveyed before that volume is large enough to contain one galaxy. This fact is used in Paper II.

3. THE GENERALIZED BIAS CORRECTION, $M_0 - M(m, v_i)$, FOR EACH DISTANCE INTERVAL

3.1. *Envelope Lines in the Spaenhauer Diagram for a Gaussian Luminosity Function*

The upper and lower envelope lines in Figure 2 (*bottom*) define the loci along which one galaxy is expected at a given redshift. The volume surveyed at redshift v in dv is proportional to $v^2\,dv$. This is the normalization factor by which the luminosity function must be multiplied to find the number of galaxies at that redshift. Larger volumes are surveyed at larger redshifts. Hence, the luminosity function must be read further into its bright and faint wings to satisfy the condition that one galaxy be found at that redshift. It is from this condition that the upper and lower envelope lines in Figure 2 (*bottom*) can be calculated when any particular analytical form of the luminosity function is adopted.

If the luminosity function is symmetrical in magnitudes, then these envelope lines will also be symmetrical relative to the apex magnitude in the bottom panel of Figure 2.

Figure 3 shows the result of a calculation using Gaussian luminosity functions with dispersions between 0.1 and 0.9 mag. That a Gaussian error function with such dispersions is realistic for S0 galaxies and for spirals is shown elsewhere (Sandage, Binggeli, & Tammann 1985, Figs. 16–19; Binggeli et al. 1988).

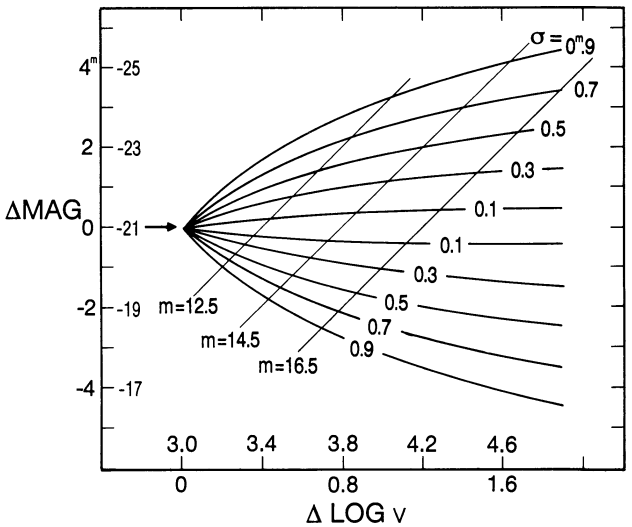

FIG. 3.—Template curves for the upper and lower envelope lines, calculated for a Gaussian luminosity function with the family of dispersions shown. The curves are universal in ΔM and $\Delta \log v$, such that they can be shifted vertically and horizontally over *any* observed distribution, such as that in Fig. 2. The arbitrary zero points of ordinate and abscissa, marked along the inner borders, permit the apparent magnitude limit lines of $m = 12.5$, 14.5, and 16.5 to be drawn using equation (4) of the text, which assumes $H_0 = 50$ km s^{-1} Mpc^{-1}.

Lines of constant apparent magnitude can be put in Figure 3 using $m - M = 5 \log v + 16.5$ for $H_0 = 50$ km s^{-1} Mpc^{-1} once absolute values of the ordinate and abscissa are adopted. With the assignment of these values, marked on the inside borders of Figure 3, the lines of constant apparent magnitude for three assumed apparent magnitude catalog limits are as shown.

Figure 3 can be used as a template (referring to the outer abscissa and ordinate scales) to slide both vertically and horizontally over any distribution of points, such as in Figure 2 (*bottom*), to determine the placement of the apex and the envelope curves in any Spaenhauer diagram.

3.2. *Two Ways to the Malmquist Ensemble Correction*

The difference between M_0 and the ensemble average, $M(m)$, that was calculated by Malmquist is shown in the bottom panel of Figure 2 by the two arrows. Two intuitive approaches in formulating methods to calculate $M_0 - M(m)$ are useful.

3.2.1. *The Method Not Used by Malmquist*

The details of Figure 3 are reproduced in Figure 4, showing vertical lines that separate the Spaenhauer diagram into redshift intervals of 0.1 dex and limit lines placed at apparent magnitudes 12.5, 14.5, and 16.5. The hatched area shows the subset of the sample that is *volume-limited* in the $m = 12.5$ case. Note that the unbiased subsample of the complete catalog moves outward in redshift for fainter apparent flux limits, showing why adding a fainter sample is the decisive diagnostic tool.

A principal feature of Figure 4 is that the sample becomes progressively more incomplete at larger redshifts. Therefore, the difference between M_0 and the proper absolute magnitude, $M(m, v_i)$, at redshift v_i, becomes progressively larger as v_i increases.

Adding a fainter sample provides a test for bias because if we

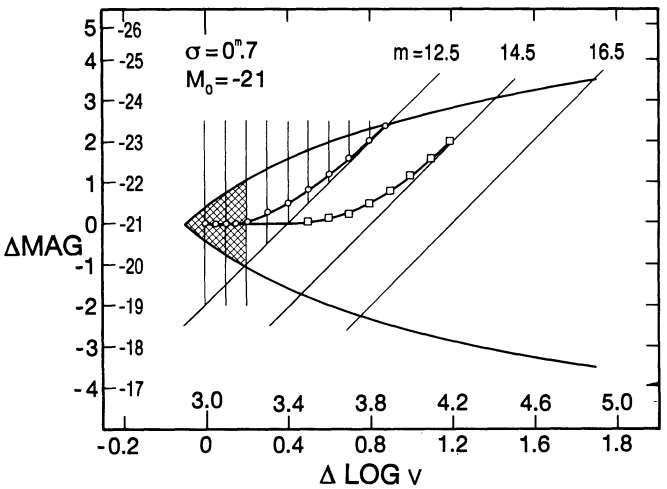

FIG. 4.—Same as Fig. 3, but with vertical lines separating the parameter space into discrete redshift intervals. The unbiased, distance-limited subset of the total sample is contained within the hatched area for $m_{limit} = 12.5$. The mean absolute magnitude of the individual samples within each indicated redshift bin is shown by the curved lines, marked by circles and squares at the beginning of each bin. Note that these curves are isomorphic, shifted in redshift by 0.4 dex for the 2 mag difference in the value of the apparent magnitude limits adopted here for display purposes.

change the apparent magnitude limit faintward, the incompleteness levels become the same as they were at brighter magnitudes but at 1 mag fainter for every 0.2 increase in $\log v_i$. This is the prediction that can be tested in any sample *if the effect is due to selection bias.*

The distribution of the absolute magnitudes within any particular vertical redshift bin in Figure 4 has, of course, the shape of the luminosity function. However, the normalization factor is different in each bin, increasing with redshift by 0.6 dex per change of 0.2 dex in redshift interval. This is simply the increase in the volume factor with increasing redshift for uniform space density.

Integration of the absolute magnitude downward, weighted by the luminosity function in each bin, gives the mean absolute magnitude of the sample *in that redshift interval.* The integration is, of course, stopped at the apparent magnitude limit line. The resulting mean value of the absolute magnitude of the truncated distribution is the mean absolute magnitude, $M(m, v_i)$, *at that redshift* and is the correction we seek.

The ensemble mean, $M(m)$, for the *complete* sample is what Malmquist calculated. It is simply the average of all individual $M(m, v_i)$ values over all redshifts, weighted by the individual volume factors. Hence, a way to obtain $M(m)$ is to sum the separate weighted integrations for $M(m, v_i)$ horizontally in Figure 4, i.e., over all redshifts. The calculation is, then, the double integral within the permitted limit lines, stopped progressively at brighter absolute magnitudes at higher redshifts by the appropriate sloping apparent magnitude catalog limit line.

The $M(m, v_i)$ values in each redshift bin are shown as circles and squares in Figure 4 for the limit lines at $m = 12.5$ and 14.5, respectively. The luminosity function was assumed to be Gaussian with $M_0 = -21$ and $\sigma = 0.7$ mag. The space density was assumed to be constant for the particular calculation of the mean lines in Figure 4.

Note again that these curves of mean absolute magnitude, $M(m, v_i)$, are shifted isomorphically to larger redshifts by 0.2

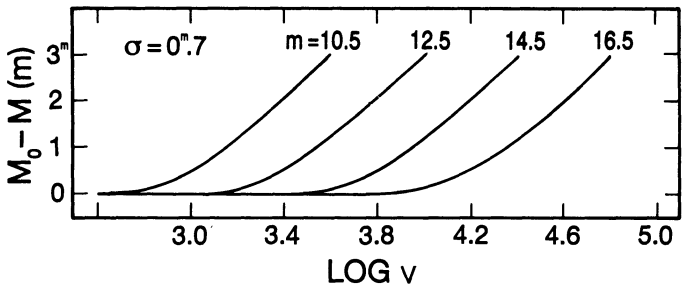

FIG. 5.—Summary of the correction to be applied to M_0 at each redshift for complete samples that are progressively flux-limited at four different limiting apparent magnitudes. The curves apply for the special case of $M_0 = -21$ for a Gaussian luminosity function with $\sigma = 0.7$ mag. The general case for any value of M_0 is set out in Table 1.

dex in redshift per unit change in the limiting magnitude. The details of this shift are shown in Figure 5, where the results of the bin-by-bin (vertical) integrations are displayed.

Later in this section we give an analytical calculation that generates the curves in Figure 5 for any assumed dispersion and redshift interval (Fig. 8 and Table 1 below). The special case of $\sigma = 0.7$ mag is shown in Figure 5.

We finish this subsection by showing the result of summing the individual numerical bin integrations horizontally in Figure 4 to obtain the Malmquist ensemble average, $M(m)$, of the sample. Figure 6 shows the details of this "granular" numerical calculation just described, using the gross redshift interval of 0.2 dex for the vertical bins of Figure 4. A limit line at apparent magnitude $m = 14.5$ has been assumed, again with a Gaussian luminosity function with an apex magnitude of $M_0 = -21$ and $\sigma = 0.7$ mag.

The separate absolute magnitude distributions within each of the six discrete redshift $\log v$ intervals 3.2–3.4, 3.4–3.6, 3.6–

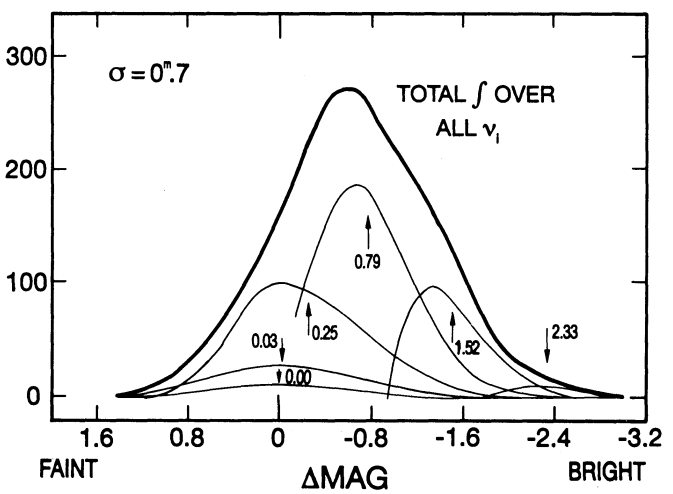

FIG. 6.—Distribution of absolute magnitudes in discrete redshift bins in the model shown in Fig. 4. The six redshift intervals for the distributions shown as thin lines are, from left to right, for $\log v$ values between 3.2 and 3.4, 3.4 and 3.6, 3.6 and 3.8, 3.8 and 4.0, 4.0 and 4.2, and 4.2 and 4.4. The mean absolute magnitude differences from M_0 for each bin are shown by arrows. These differences range from 0 mag for the distance-limited part of the sample in the range $\log v = 3.2$–3.4, to 2.33 mag for the redshift bin in the range $\log v = 4.2$–4.4. The distribution of absolute magnitude for the entire flux-limited sample is the heavy overriding curve. It has a maximum that is 0.68 mag brighter than the M_0 value for the true (distance-limited) luminosity function, which is the zero point of the abscissa.

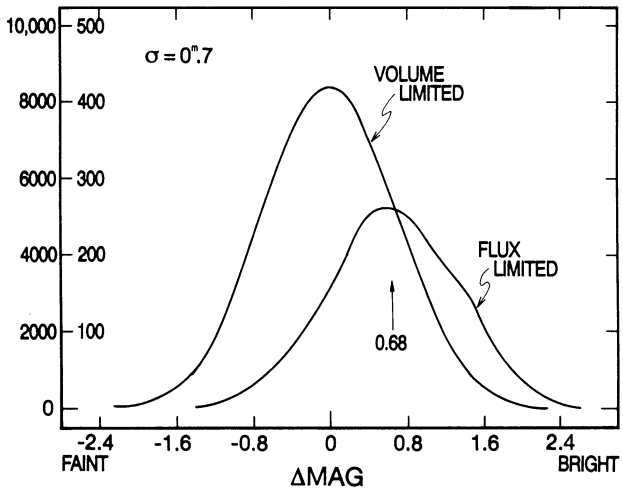

FIG. 7.—Comparison of the true (distance-limited) assumed luminosity function used for the calculation in Fig. 6 with the flux-limited distribution copied from the overriding curve in Fig. 6. The difference between M_0 and $M(m)$ of 0.68 mag is indicated for this special case of $\sigma(M) = 0.7$ mag.

3.8, 3.8–4.0, 4.0–4.2, and 4.2–4.4 are shown in Figure 6, drawn with thin lines under the total distribution that is given by the overriding heavy line. Shown by a series of arrows are the calculated mean absolute magnitude corrections, $M_0 - M(m, v_i)$, for the same six redshift intervals. For example, the mean correction to M_0 is 1.52 mag for the log redshift interval of 4.0–4.2, shown under the truncated Gaussian distribution valid for that redshift interval.[4]

The thin curves in Figure 6 are properly normalized in absolute frequencies by the volume factors for the various redshift intervals for a homogeneous space distribution.

The sum of the individual distributions over the available parameter range is the heavy, overriding curve in Figure 6. This is the distribution of absolute magnitudes of the complete flux-limited sample, i.e., the distribution of absolute magnitudes only for those galaxies that appear in a complete flux-limited catalog. Note again that Figure 6 is for the special case of $m(\text{limit}) = 14.5$, $M_0 = -21.0$, and $\sigma(M) = 0.7$.

The comparison between the true distribution of absolute magnitudes (i.e., in a volume-limited sample) and the distribution in the flux-limited catalog is shown in Figure 7. The curve on the right is the top curve from Figure 6. The curve marked "volume limited" is the true Gaussian luminosity distribution. The numbers on the outside of the ordinate border are for the volume-limited sample. Those on the inside are for the flux-limited distribution.

The shift in the mean absolute magnitude defined by the two distributions is 0.68 mag, as found from these numerical integrations. Note that this is the same value (as of course it must be if our procedure is correct) as obtained from the analytical derivation of $M_0 - M(m) = 1.386\ \sigma^2$ from this Malmquist (1920) equation if $\sigma = 0.7$ mag.

[4] The left-hand parts of each separate distribution of the truncated Gaussians for each redshift interval are not exactly vertical in Figure 6 for the *high*-redshift intervals. Here the sample is flux-limited. Had we passed to the limit of an infinitesimal redshift interval at these at these high redshifts, the left edges of the distribution shown in Fig. 6 would have been strictly vertical, i.e., with a sharp cutoff. However, for the lowest redshift intervals, the apparent distributions remain nearly Gaussian because the data there are more nearly distance-limited (galaxies in both the bright and faint wings of the Gaussian exist in the catalog).

We have made the calculation with considerable pedantry to this point (numerically in finite redshift bins), to help the intuition for the passing to the limit of infinitesimal redshift intervals, as follows.

Generalizing the previous method gives a way to calculate a "universal" set of the fundamental $M(m, v_i)$ bias-free absolute magnitudes, which we seek at every redshift v_i in dv_i for any value of $\sigma(M)$, and for any catalog flux limit m. Refer again to Figure 4 (also the inset in Fig. 8 below). Collapse the redshift bin to a vertical line at some redshift v_i. Along this line the galaxies are distributed with any adopted luminosity distribution. For the demonstration here we again consider the function to be Gaussian. We seek the *mean* absolute magnitude of the distribution *along a particular vertical line*, i.e., at a particular redshift v_i, where the distribution is progressively terminated at the place where the vertical line meets a particular apparent magnitude limit line such as $m = 12.5$ or 14.5 in Figure 4.

Consider this progressive termination of the integration at faint absolute magnitudes as we move the vertical line to smaller redshifts. The mean absolute magnitude, $M(m, v_i)$, of the distribution at v_i moves closer to M_0 as the vertical line approaches that redshift which separates the distance-limited region from the flux-limited region in Figure 4. For all redshifts smaller than this, the mean absolute magnitudes of the subsamples are, of course, M_0 because the sample is complete within a given volume.

The value of $M(m, v_i)$ along any given vertical line at redshift v_i can be calculated by truncating the Gaussian at various values of the $t = (M_0 - M)/\sigma$ parameter and appropriately integrating under the remaining partial Gaussian. The Gaussian luminosity function is assumed to be

$$\text{erf}\,(t) = A_i(2\pi)^{-0.5} \exp\,(-0.5t^2)\,, \qquad (1)$$

where A_i is the volume normalization factor at redshift v_i, and where

$$t(v_i) = [M_0 - M(m, v_i)]/\sigma\,. \qquad (2)$$

The mean value of t when the Gaussian is truncated by the straight catalog limit line is given by

$$\langle t \rangle = \frac{\int_{t(\text{limit})}^{+\infty} t\ \text{erf}\,(t)dt}{\int_{-\infty}^{+\infty} \text{erf}\,(t)dt}\,. \qquad (3)$$

Here the upper limit in the numerator is from infinitely bright luminosities, and the lower limit is the t-value at the lower termination. The denominator is simply the total number in the sample at redshift v_i in the interval dv_i.

The absolute magnitude at the intersection of the vertical line at redshift v_i with the fixed catalog limit, m_{limit}, is

$$M(v_{i,\text{limit}}) = m_{\text{limit}} - 5\ \log\ v_i - 16.50\,. \qquad (4)$$

From this, the value of t at this intersection is $t = [M_0 - M(m, v_{i,\text{limit}})]/\sigma$ (see the inset in Fig. 8 below).

Table 1 shows the result of an integration similar, but not identical, to that of equation (3). For the table we have integrated the Gaussian numerically, not from $t = \pm\infty$, but starting only at $t = 3.4$. Yet this is far enough into the Gaussian wings so that the integration is numerically complete to within ~1%. To this extent, Table 1 is "universal" (see footnote 6 at the end of this section).

TABLE 1

UNIVERSAL BIAS CORRECTION FOR A GAUSSIAN LUMINOSITY FUNCTION

BRIGHT SEGMENT		FAINT SEGMENT	
$t=(M_0-M_{v,1})/\sigma$ (1)	$[M_0-M(m)]/\sigma$ Bias Correction (mag) (2)	$t=(M_0-M_{v,1})/\sigma$ (3)	$[M_0-M(m)]/\sigma$ Bias Correction (mag) (4)
3.4	3.40	0.0	0.74
3.2	3.27	−0.2	0.62
3.0	3.12	−0.4	0.51
2.8	2.96	−0.6	0.41
2.6	2.80	−0.8	0.33
2.4	2.62	−1.0	0.25
2.2	2.45	−1.2	0.19
2.0	2.28	−1.4	0.14
1.8	2.11	−1.6	0.10
1.6	1.94	−1.8	0.07
1.4	1.77	−2.0	0.04
1.2	1.61	−2.2	0.03
1.0	1.45	−2.4	0.02
0.8	1.29	−2.6	0.01
0.6	1.14	−2.8	0.005
0.4	1.00	−3.0	0.002
0.2	0.86	−3.2	0.0008
0.0	0.74	−3.4	0

Table 1 shows $\langle t \rangle$ for any given $(t_{i,\text{limit}})$ when the Gaussian is defined only for $t < 3.4$, as in the last paragraph. Columns (1) and (3) are the t_i values, above which galaxies exist in the sample (i.e., above the lower apparent magnitude limit line in Fig. 4 at a particular redshift v_i). Columns (2) and (4) show the mean $[M_0 - M(m, v_i)]/\sigma$ value, which is the correction we seek. The left and right sections of the table separate the parts of the distribution for which the $M(v_{i,\text{limit}})$ values are respectively brighter and fainter than M_0.

An example illustrates how Table 1 is used to find the bias correction to M_0. For this example let $M_0 = -21.0$ and $\sigma = 0.7$ mag as in Figure 5, and let the catalog limit of a particular sample be at $m = 12.5$.

If we seek the value of the proper mean absolute magnitude required for galaxies at the redshift $\log v_i = 3.8$, then equation (4) with $\log v_i = 3.8$ gives $M_{v,\text{limit}} = -23.0$ for $m = 12.5$. This absolute magnitude, defined as the M-value at the intersection of the $m = 12.5$ limit line with the vertical redshift line at $v_i = 3.8$ in Figure 4, is 2.0 mag brighter than $M_0 = -21.0$. Using the definition that $t = [M_0 - M(m, v_i)]/\sigma$ with $\sigma = 0.7$ mag, the $(t_{i,\text{limit}})$ value is $2.0/0.7 = 2.86$. This is the $(t_{i,\text{limit}})$ value at the lower termination point to be used in Table 1, giving $[M_0 - M(m, v_i)]/\sigma = 2.99$ at this t_{limit} value on the faint side of the Gaussian. The bias correction from this table is then $M_0 - M(m, v_i) = 2.99 \times 0.7 = 2.09$ mag at $\log v = 3.8$. This is the same value shown in Figure 5 that was obtained from the direct numerical integration at that redshift, verifying the procedure.

The results in Table 1 are presented graphically in Figure 8, showing again the definition of $M_{v,\text{limit}}$ for any arbitrary redshift v_i.

3.2.2. *The Method Used by Malmquist to Obtain $M_0 - M(m)$*

The second, conceptually easier, way to calculate the Malmquist ensemble correction, $M_0 - M(m)$, is shown in Figure 9. As in Figure 4, the three variables are still redshift, absolute magnitude, and apparent magnitude, but the generator of the family of curves is now M rather than m. Said differently, lines

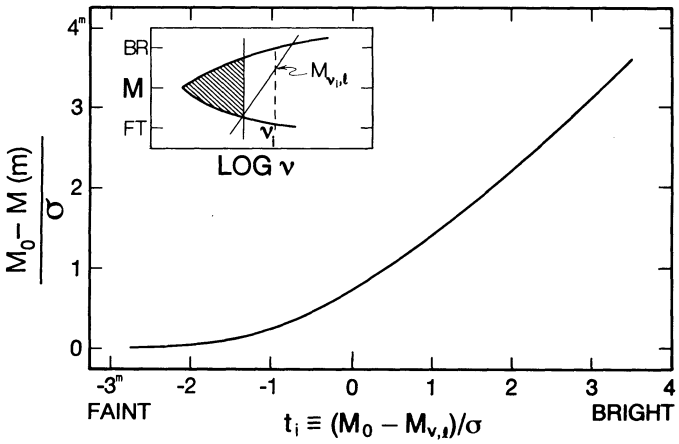

FIG. 8.—"Universal" correction to M_0 from Table 1 for a Gaussian luminosity function with arbitrary dispersion, for any redshift and any adopted apparent magnitude limit to a given catalog. The curves in Fig. 5 are special cases of this function calculated for the M_0, σ, $\log v$, and m_{limit} values given there. See the caveat in footnote 6.

of constant m are the curves internal to the axes in Figure 4, whereas lines of constant M generate the family in Figure 9. The relations between the variables are again given by equation (4).

Figure 9 sets out a method that is equivalent to that developed by Kapteyn to solve the fundamental equation of stellar statistics by numerical methods. Note that Figure 9 is in fact a classic $(M, \log \pi)$ table (Bok 1937, p. 28).

The calculation begins by dividing the volume into a number of spherical shells and determining the number of objects in each shell at distance r in interval dr with absolute magnitude M in interval dM that contribute to the objects observed at apparent magnitude m in dm. Figure 9 is a spreadsheet that solves the famous equation connecting these variables by making the volume shells discrete, separated by intervals of 0.2 in the log of the distance. As in Figure 4, this gives apparent magnitude intervals separated by 1 mag in m, shown along the abscissa of Figure 9. Lines of constant absolute magnitude, calculated from equation (4), thread the diagram as shown. The volume between successive 0.2 dex intervals of the ordinate increases as 0.6 dex, or factors of 3.96, as in Figure 4. This is the normalization factor by which each entry from the luminosity function in each box (such as A and B) must be multiplied to obtain the number density in that box.

The two volume intervals (hatched areas in Fig. 9) are between log redshifts of 3.2 and 3.4, and 3.6 and 3.8 (read along the right-hand ordinate). The ratio of volumes for these two particular redshift intervals is 15.8. The ratio of the two numbers in the A and B boxes is then 15.8 multiplied by the ratio of the luminosity function at absolute magnitudes -20 and -22.

Summing the entries in each box, calculated in this way, vertically (i.e., over all distances to infinity), say in the column containing boxes A and B, gives $A(13)$, which is the total number of objects that will be observed between apparent magnitudes $m = 12.5$ and 13.5 (read along the top abscissa) per unit area on the sky.

The Malmquist calculation of $M(m)$ is found as the *mean* absolute magnitude of the subset of objects summed and averaged over the *vertical* columns of Figure 9, stopped at the right at a given catalog cutoff magnitude.

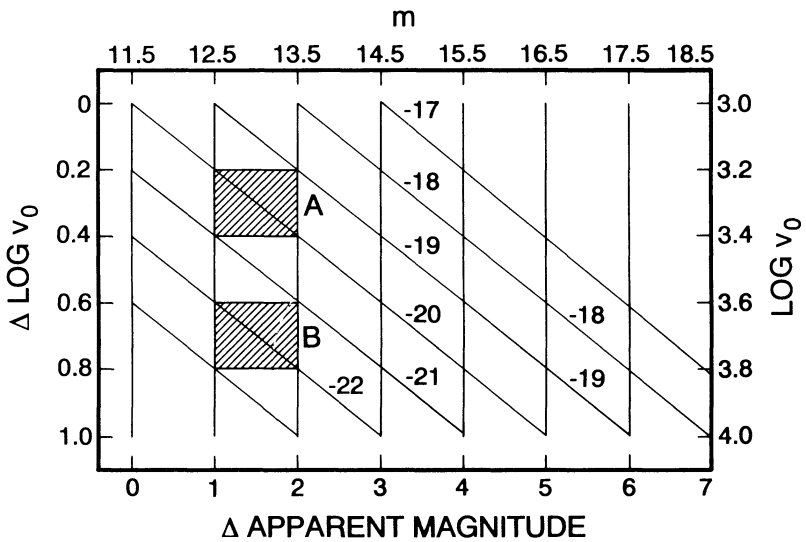

FIG. 9.—Spreadsheet illustrating the method of calculating the classical Malmquist equation for the mean absolute magnitude, $M(m)$, of a sample that is complete to a given apparent magnitude. The diagram sets up the (M, log π) method for solving the fundamental equation of stellar statistics numerically. The $M(m,v_i)$ values are obtained by summing the *rows* (not shown by horizontal lines) at a given redshift interval between v_i and v_j, where that interval is 0.2 dex in the diagram. The Malmquist ensemble mean, $M(m)$, is found by averaging the boxes over the relevant parameter space of the diagram.

If the volumes did not increase downward in each vertical column, this mean value would be simply M_0. However, because the volume elements *do* increase downward at the rate of 3.98 per 0.2 interval in log v, the brighter absolute magnitudes (toward the bottom of each column) are weighted more heavily than the fainter. This means that the ensemble average over all absolute magnitudes in a complete sample (to apparent magnitude m) gives a mean absolute magnitude that is brighter than M_0. Malmquist's (1920) integration to obtain $M_0 - M(m)$ is equivalent to finding the mean of all the numbers in all the boxes brighter than m(limit).

By a different elegant analytical procedure, he obtained

$$M_0 - M(m) = 2.31\ \sigma^2\, d\ \log\ A(m)/dm\ , \qquad (5)$$

if the luminosity function is Gaussian with dispersion σ. For a homogeneous distribution of objects in space, $d\ \log\ A(m)/dm = 0.6$. The famous Malmquist mean correction is then

$$M_0 - M(m) = 1.386\ \sigma^2\ . \qquad (6)$$

for this case of *uniform space density*.

Study of Figure 9 shows that equations (5) and (6) are valid for *each* finite apparent magnitude interval. They are therefore valid for the complete apparent magnitude interval from the brightest in the catalog to m(limit). This can be understood by noting that the entries in each box in each vertical column are taken from the *same* luminosity function, but simply displaced up or down relative to adjacent columns, and further that the weighting functions (i.e., the volume elements) are isomorphic relative to the luminosity function. Therefore, a summing of the vertical columns to infinity, i.e., over all vertical boxes, gives the same answer for $M(m)$, i.e., the *mean* absolute magnitude *in each column*. The method via Figure 9 also makes clear why the Malmquist ensemble mean, $M(m)$, is the result of integrating over all distances[5] (i.e., from 0 to ∞).

However, as emphasized throughout this paper, the bias correction we need is not $M(m)$ but the $M_0 - M(m, v_i)$ value at each redshift. This is obtained by *summing the boxes in Figure 9 horizontally* up to m(limit) in a given redshift interval. Note that the numerical integration done in this way in Figure 9 is equivalent to what we did via Figure 4, and is, of course, replaced by the continuum calculation set out in Table 1 (Fig. 8).

We finally inquire how restrictive the results of Table 1 are to the assumption of a Gaussian luminosity function. Clearly, the methods we use in this paper can be applied for any arbitrary luminosity function. Spaenhauer has made a Monte Carlo simulation of the equivalent of Figures 3 and 4 using a Schechter function as well as a Gaussian. The results, given graphically elsewhere (Tammann & Sandage 1982, Fig. 2), show that the difference is minor, and therefore that the results in Table 1 are robust.[6]

4. ADDING A FAINTER S0 + Sa SAMPLE

In the previous sections we have emphasized that observational selection bias can always be detected by adding a fainter sample of objects of the same type to a Spaenhauer diagram. If selection bias is present, the apparent correlation of M with redshift in a diagram such as that in the top panel of Figure 2

[5] Of course, the luminosity function goes to zero over much of the very near and the very distant parameter space in Fig. 9. This was expressed in Fig. 4 by keeping within the upper and lower curved limit lines. No such limit lines are drawn in Fig. 9, although they exist. Integrating over *all* distances by extending the column length to infinity in Fig. 9 is equivalent to integrating over *all* redshifts in the parameter space in Fig. 4 that are to the left of the flux limit lines, i.e., by neglecting the upper and lower limit lines in Fig. 4. But again, of course, the luminosity function does go to zero over much of this complete parameter space, both in Fig. 4 and in Fig. 9.

[6] A final caveat is necessary. As mentioned previously, Table 1 is calculated for a Gaussian luminosity function stopped at the bright and faint end at $t = \pm 3.4$. The rigorously *correct* calculation of $\langle t \rangle$ for *any* Spaenhauer configuration at any redshift *should start the integration at the t-value that applies only to the upper envelope curve*, and then to stop at the magnitude limit line of a particular catalog at the faint end. The difference between this and what has been done for Table 1, where the fixed limits of $t = \pm 3.4$ are used, is only a few hundredths of a magnitude. This is negligible; the calculations in Federspiel et al. (1994) (Paper III) are, however, exact on this point.

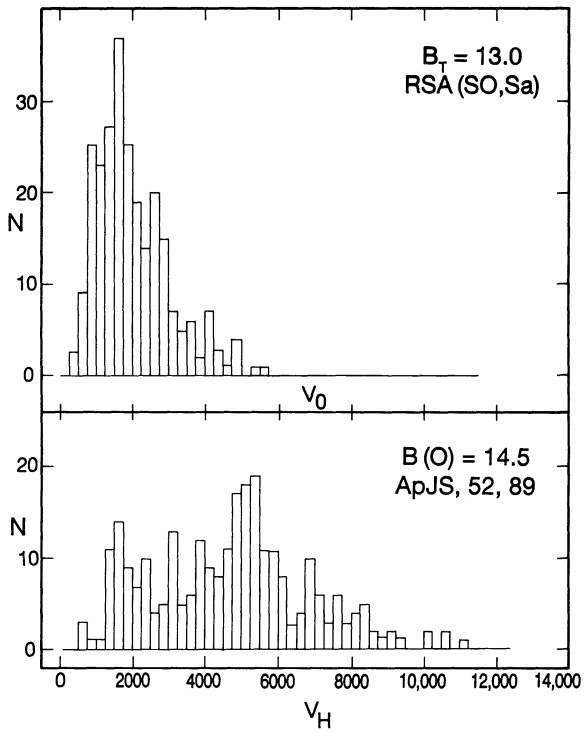

FIG. 10.—Distribution of redshifts for S0 + Sa galaxies in the RSA (*top*) and in the deeper catalog of Huchra et al. (1983) between R.A. = 0^h–10^h and R.A. = 14^h–24^h (*bottom*).

will move to larger redshifts by an amount of 0.2 in log v for a 1 mag increment in the faint flux limit.

We make this experiment in a way similar to that using Sc I galaxies (S88a), but using here S0 + Sa galaxies, again as in Figure 2 (*top panel*), but now with a fainter sample. The added sample is from the redshift catalog of Huchra et al. (1983, hereafter HDLT), which contains 2401 galaxies of all types, most of which are fainter than those in the RSA. The listed apparent magnitude limit of the HDLT catalog is $B(0) = 14.5$, where $B(0)$ is the apparent magnitude on a system of isophotal magnitudes used in the Zwicky et al. catalogs. The zero point of this system is fainter by 0.3–0.4 mag than that of the B_T system used in Figure 2*b* (Huchra 1976; RSA1, RSA2, p. 131). Adopting a correction for the $B_T - B(0)$ difference to be 0.3 mag gives a statistical magnitude limit of $B_T = 14.2$ for the HDLT catalog. This is 1.2 mag fainter than the magnitude limit of the RSA.

Galaxies with listed morphological types between $T = -2$ and $T = +1$ (corresponding to Hubble types between S0 and Sa) in the fainter catalog were selected between right ascensions 0^h–10^h and 14^h–24^h, avoiding the Local Supercluster.

Figure 10 shows that the redshift distribution of the subsample of 263 such galaxies reaches larger redshifts than does the RSA, verifying that the condition for larger distances is met for the test we propose here of adding a fainter sample.

Figure 11 shows that the distribution of added points in a Spaenhauer diagram does indeed move *toward larger redshifts*, rather than continuing the trend toward brighter M as in Figure 2 (*top*). By the argument we have been making, this

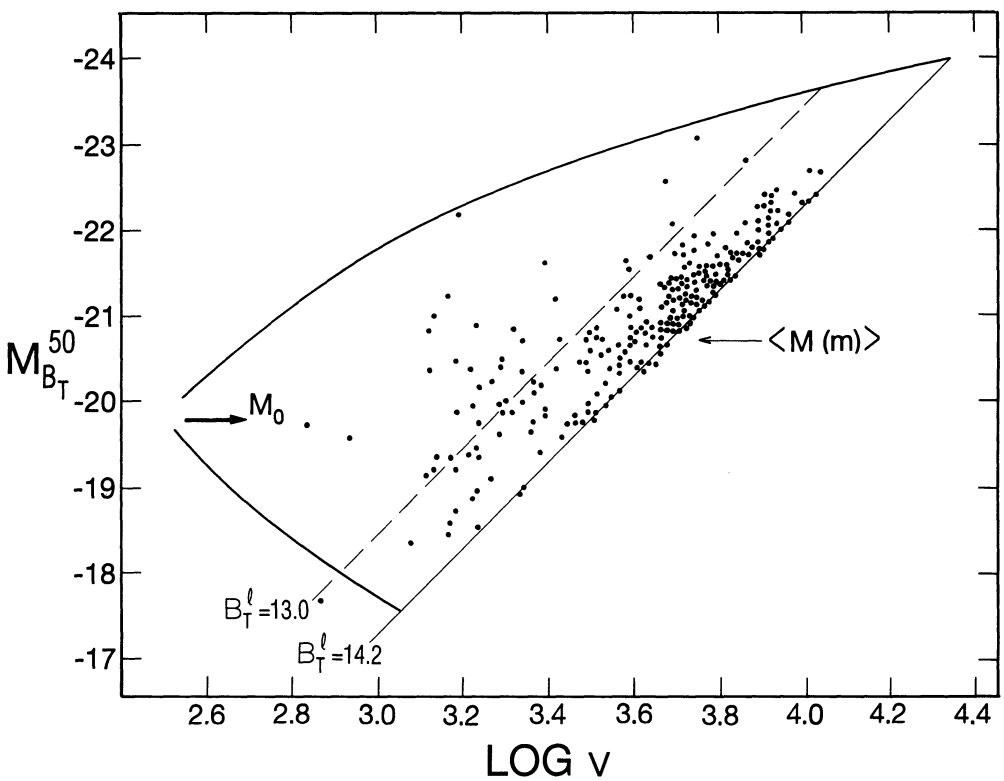

FIG. 11.—Result of adding the fainter Huchra et al. sample for S0 + Sa galaxies to Fig. 2 (*bottom panel*). The positions of the M_0 and $M(m)$ arrows are the same as in Fig. 2.

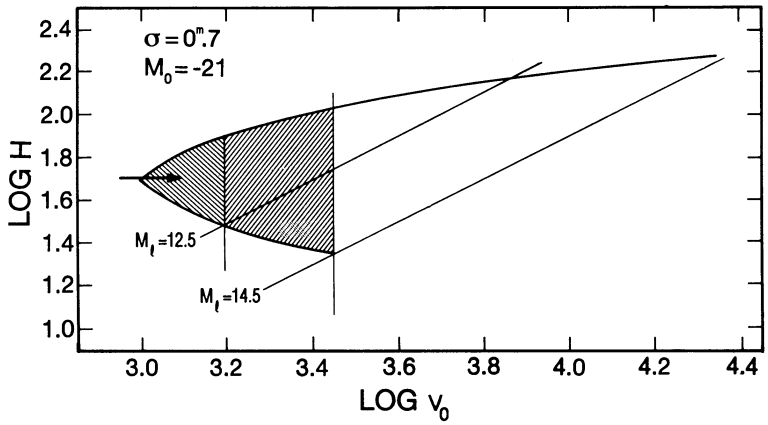

FIG. 12.—Effect of incomplete samples on the determination of the mean Hubble constant. The correct mean value of log H_0 is obtained only within the hatched areas for the two assumed limiting apparent magnitudes. An arbitrary value of $H_0 = 50$ km s^{-1} Mpc^{-1} is assumed for the vertical position of the apex in the distance-limited part.

proves the presence of selection bias rather than a real effect of H_0 increasing outward.[7]

5. THE HUBBLE CONSTANT DOES NOT INCREASE OUTWARD

The point of this paper is that if a fixed value of the mean absolute magnitude (say M_0) is used to determine photometric distances to galaxies such as those in the samples in Figures 2 (*bottom panel*) and 11, then *systematic errors will be made in the distances that depend on true distance*, and therefore that a false appearance of the Hubble constant increasing outward will be perceived. To avoid this progressive distance-scale error it is necessary to use the double-entry $M(m, v_i)$ correction in Table 1 at every redshift.

The consequence of neglect of this correction is as follows. If a *fixed* mean absolute magnitude, M_0, is used for each object, then the distribution of apparent Hubble parameters, one for each object, will fill the area between the boundaries of Figure 12. (Two apparent magnitude limits are shown in Figs. 12 and 13.) The correct *average* value of log H_0 will only be obtained from the distribution within the hatched areas that define the distance-limited subset of the data. That part of the sample which is at higher redshifts imitates a mean Hubble constant that (incorrectly) increases outward in the nonhatched areas of both Figures 12 and 13.

Figure 13 (*bottom panel*) shows the *mean* value of H_0 that would be obtained at every redshift when using a sample whose data would fill the area outlined in the top two panels in Figure 13. These mean loci are similar to the mean curves that thread the Spaenhauer diagram as, for example, in Figure 4.

[7] The difference between the position of the $M(m)$ arrow in the bright and the faint sample in Fig. 11 and the position in Fig. 2 is, we believe, due to the inhomogeneous distribution of redshifts in this redshift range (Giovanelli & Haynes 1991, Figs. 1a, 1b, 1c) rather than to a failure of the model. $M(m)$ *should* be independent of the apparent magnitude limit, m. This is shown by the ideal model set out in this paper, made implicit in Fig. 9, and by the discussion of it earlier.

The inhomogeneity of the space distribution of the galaxies in the new sample in Fig. 11 is seen from the abnormal shape of the redshift distribution in Fig. 10 (*bottom*), showing the effect of the large Perseus-Pisces density enhancement at 5000 km s^{-1}. The effect of such an enhancement on mean absolute values, similar to the bunching of points in Fig. 11 near log $v = 3.7$, is seen in the original simulations by Spaenhauer (Tammann & Sandage 1982, Fig. 2), mentioned earlier.

Figure 13 (*bottom panel*) shows why adding a fainter sample increases the redshift limit within which a correct (bias-free) value of H_0 could be determined. For redshifts beyond the hatched boundary, the derived values of H_0(apparent), using a fixed M_0 value, will be too large, *and will be multivalued* depending on the catalog limit. This is clearly a contradiction. However, using the double-entry bias-free $M(m, v_i)$ absolute magnitudes determined from Table 1 removes both the apparent increase of H_0 outward (de Vaucouleurs & Peters 1986) and the multivalued dependence of H_0 on the catalog limiting magnitude.

That the Hubble constant does not increase outward is seen from the comparison of Figures 2 (*top*) and 11 using S0 and Sa

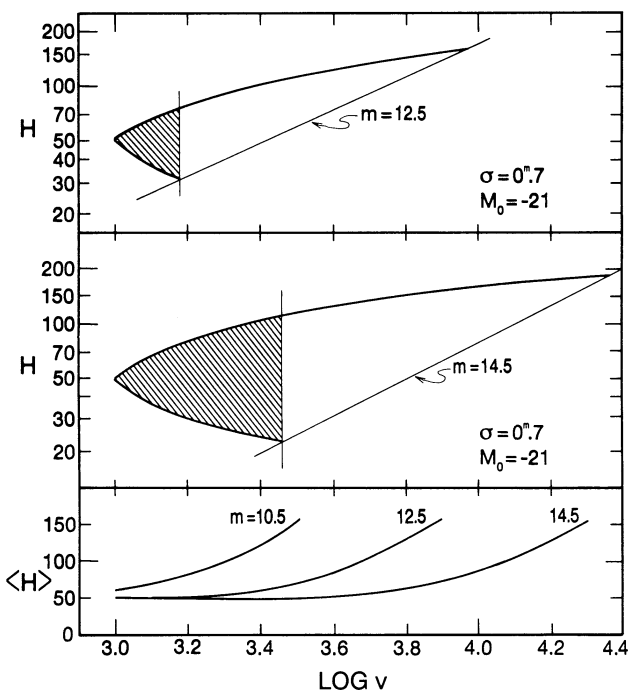

FIG. 13.—Same as Fig. 12, but showing the effect for each limiting catalog magnitude separately. The bottom panel shows that the derived mean Hubble constant will appear to be multivalued when two catalogs with different flux limits are compared that have not been corrected by Table 1.

galaxies. Earlier data, both for Sc I galaxies (S88a) and of a different kind (Sandage, Tammann, & Hardy 1972; Sandage & Tammann 1975, Fig. 6; Sandage 1975, Figs. 4 and 5; Sandage 1992) have led to the same conclusion.

The more complicated case of selection bias in data samples that have been analyzed by the Tully-Fisher distance method is developed in Paper II immediately following, using a method that generalizes the present paper. It is shown there that the apparent increase of H_0 outward (Giraud 1985, 1986*a*, *b*, *c*; Tully 1988), when these more complicated data are improperly corrected for selection bias of the type discussed here, is also false.

The purpose of the present paper has been to provide a necessary preparation for the much more complicated, but also much more important, case that uses the Tully-Fisher method of distance determination, as set out in Papers II and III that follow.

The first several drafts of this paper were written at the Astronomical Institute of the University of Basel. I am grateful to G. A. Tammann for the hospitality of the Institute and for many conversations about the general problems of observational selection bias over the past two decades. I am also grateful to him for his reading of a late draft when this paper was moderately close to its present form, and for his central scientific suggestions concerning it. It is also a pleasure to thank Elizabeth Doubleday for her superior editing of the later drafts using her expertise in English grammar and conventions.

REFERENCES

Aaronson, M., et al. 1982, ApJS, 50, 241
Binggeli, B., Sandage, A., & Tammann, G. A. 1988, ARA&A, 26, 509
Bok, B. J. 1937, The Distribution of Stars in Space (Chicago: Univ. Chicago Press)
Bottinelli, L., Gouguenheim, L., Paturel, G. H., & Teerikorpi, P. 1986a, A&A, 156, 157
———. 1986b, A&A, 166, 393
———. 1988, ApJ, 328, 4
de Vaucouleurs, G., & Peters, W. L. 1986, ApJ, 303, 19
Federspiel, M., Sandage, A., & Tammann, G. A. 1994, ApJ, 430, 29 (Paper III)
Giovanelli, R., & Haynes, M. P. 1991, ARA&A, 29, 499
Giraud, E. 1985, A&A, 153, 125
———. 1986a, ApJ, 301, 7
———. 1986b, ApJ, 309, 312
———. 1986c, A&A, 174, 23
Hoffleit, D. 1982, The Bright Star Catalogue (New Haven: Yale Univ. Obs)
Huchra, J. 1976, AJ, 81, 952
Huchra, J., Davis, M., Latham, D., & Tonry, J. 1983, ApJS, 52, 89 (HDLT)
Jerjen, H., & Tammann, G. A. 1993, A&A, 276, 1
Kraan-Korteweg, R. C. 1986a, A&AS, 26, 509
———. 1986b, A Catalog of 2810 Nearby Galaxies (Basel Publ. Ser., No. 18)
Kraan-Korteweg, R. C., Cameron, L. M., & Tammann, G. A. 1986, in Galaxy Distances and Deviations from Universal Expansion, ed. B. F. Madore & R. B. Tully (Dordrecht: Reidel), 65
———. 1988, ApJ, 331, 620
Kraan-Korteweg, R. C., Sandage, A., & Tammann, G. A. 1984, ApJ, 283, 24
Lauer, T. R., & Postman, M. 1992, ApJ, 400, L47
Malmquist, G. 1920, Lund Medd., Ser., 2, No. 22
Mathewson, D. S., Ford, V. L., & Buchhorn, M. 1992, ApJS, 81, 413
Mihalas, D., & Binney, J. 1981, in Galactic Astronomy (San Francisco: Freeman), chap. 4
Sandage, A. 1972a, ApJ, 178, 1
———. 1972b, ApJ, 178, 25
———. 1975, ApJ, 202, 563
———. 1988a, ApJ, 331, 583 (S88a)
Sandage, A. 1988b, ApJ, 331, 605 (S88b)
———. 1992, Phys. Scripta, T43, 22
———. 1993a, ApJ, 402, 1
———. 1993b, ApJ, 404, 419
———. 1994, ApJ, 430, 13 (Paper II)
Sandage, A., Binggeli, B., & Tammann, G. A. 1985, AJ, 90, 1759
Sandage, A., & Hardy, E. 1973, ApJ, 183, 743
Sandage, A., & Tammann, G. A. 1975, ApJ, 196, 313
———. 1976, ApJ, 210, 7
———. 1981, 1987, A Revised Shapley-Ames Catalog of Bright Galaxies (Carnegie Inst. Washington Publ. 635) (RSA1, RSA2)
———. 1990, ApJ, 365, 1
———. 1993, ApJ, 415, 1
Sandage, A., Tammann, G. A., & Hardy, E. 1972, ApJ, 172, 253
Sandage, A., Tammann, G. A., & Yahil, A. 1979, ApJ, 232, 352 (STY79)
Segal, I. 1982, ApJ, 252, 37
Spaenhauer, A. 1978, A&A, 65, 313
Tammann, G. A. 1986, in 13th Texas Symposium, Relativistic Astrophysics, ed. M. P. Ulmer (Singapore: World Scientific), 8
———. 1987, in IAU Symp. 124, Observational Cosmology, ed. A. H. Hewitt, G. R. Burbidge, & L. Fang (Dordrecht: Reidel), 151
———. 1991, in Observational Tests of Cosmological Inflation, ed. T. Shanks, A. J. Banday, R. S. Ellis, C. S. Frenk, & A. W. Wolfendale (Dordrecht: Kluwer), 179
———. 1993, Phys. Scripta, T43, 31
Tammann, G. A., & Sandage, A. 1982, in Highlights Astron., Vol. 6, ed. R. M. West (Dordrecht: Reidel), 301
———. 1985, ApJ, 294, 81
Teerikorpi, P. 1975a, A&A, 45, 117
———. 1975b, Observatory, 95, 105
———. 1984, A&A, 141, 407
———. 1987, A&A, 173, 39
———. 1990, A&A, 234, 1
Tully, R. B. 1988, Nature, 334, 209